Desalination and Water Treatment
www.deswater.com
doi: 10.1080/19443994.2015.1020512

57 (2016) 8127–8138
April

Taylor & Francis
Taylor & Francis Group

Study on the desalination of high hardness water by electrodeionization reversal

Guang Yang, Yonggang Zhang*, Shan Guan

School of Environmental and Chemical Engineering, Tianjin Polytechnic University, Tianjin 300387, P.R. China, Tel. +86 022 83955115; Fax: +86 022 83955451; emails: yg083002@163.com (G. Yang), zhangdm0905@163.com (Y. Zhang), guanshan69@163.com (S. Guan)

Received 1 August 2014; Accepted 13 February 2015

ABSTRACT

In this study, the simultaneous removal of cationic ions (Ca^{2+}, Mg^{2+}, Na^{+}, and K^{+}) from synthetic aqueous solutions using electrodeionization reversal (EDIR) was investigated. Under the condition of relatively high-concentration influent, characteristic curves of *V–I* and *R–I* were plotted at first and the polarity reversal period of 60 min or shorter was determined based on the resistance–time (*R–T*) relationship. Effects of various operation parameters including dilute flow rates (15, 30, 60, and 90 mL min^{-1}) and cation–anion resin volume ratios (3:7, 4.7:5.3, and 7:3) were studied, respectively. The experimental results showed that the operating current of 0.85 A, dilute flow rate of 30 mL min^{-1}, and cation–anion volume ratio of 4.7:5.3 were optimal for the process performance. The average removal efficiencies of cations were more than 88% (i.e. 93.12–94.56% for Ca^{2+}, 96.21–97.14% for Mg^{2+}, 89.11–90.76% for Na^{+}, and 92.99–95.35% for K^{+}) after three repeated experiments without membrane scaling. The transport of cations through ion exchange resins was evaluated in relation to hydrated ionic radius and ionic valence. Due to various affinities of cations to the resins, the migration of divalent ions was more enhanced compared to that of monovalent ions. This study would be helpful for applying EDIR process in the treatment of high-concentration water desalination.

Keywords: Electrodeionization process; Cation ions; Polarity reversal; Water desalination; Scale; Ion migration

1. Introduction

Electrodeionization (EDI), an integration of ion exchange and electrodialysis (ED), was firstly proposed by Kunin [1] in 1950. It is a hybrid separation process for desalination under the force of direct-current electric field [2]. Compared with ED, its structural distinction is the addition of ion exchange resins packed between the cation exchange membrane (CM) and anion exchange membrane (AM). With this innovative structure, the electric conductivity is enhanced by several orders of magnitude for ionic electromigration in the compartment [3], and thus, the salt ions can be removed with a higher efficiency and lower power consumption than ED. In the EDI process, when water dissociation takes place, a significant part of electric current is carried by the ionic products of water dissociation and the resins will be electrochemically transformed into H-form and OH-form, then

*Corresponding author.

maintaining a continuous deionization process without chemical regeneration [4]. Hence, it is able to break through the limitations of ED and conventional ion exchange. As an advanced and environmental-friendly technology, it is increasingly studied and applied in different fields such as ultrapure water production [5–7], removal or recovery of heavy metal and nonmetal [8,9], purification of organic matters [10,11], and food engineering [12].

In the EDI process, hardness ions [13] such as Ca^{2+} and Mg^{2+} react with OH^-, SO_4^{2-}, or HCO_3^- to form precipitation on membrane surface, which results in the increased resistance. This phenomenon will lead to the degradation of the EDI performance. Thus, preventing the scaling of the membranes is important in the long-term operation for EDI. In order to inhibit the fouling phenomena, electrodeionization reversal (EDIR) process [14,15] was employed to overcome the problems using a method of polarity reversal of electrodes. In EDIR system, resins are all packed in the dilute compartments (DC) and concentrate compartments (CC). After the reversal of the electrodes, DC and CC are interchanged and the membrane fouling will be minimized or prevented.

In previous studies, Lee et al. [16,17] softened the water by EDIR system without scaling formation on the membrane surface and the empirical limiting current density as functions of flow rate and hardness concentration was determined. Park et al. [13] used different membrane processes (ED, EDR, and EDIR) to remove hardness ions from tap water. On these bases, EDIR showed the feasibility as a softening process. However, the EDI and EDIR processes were usually focused on the removal or recovery for only one type of ions [18,19] or demineralization of reverse osmosis permeate [20]. For high-concentration feed with multiple ions, the desalting and softening processes were rarely discussed. Under natural conditions, ions are usually coexisting and the concentration is relatively high. Hardness ions, including divalent cation species such as Ca^{2+}, Mg^{2+}, and alkali metals (Na^+ and K^+) often coexist in brackish water. Due to ionic valence, hydrated ionic radius, and affinity with resins, the removal of a particular metal ion will be affected by the presence of other metal ions.

Thus, the purpose of this study was to investigate the desalting process of high-concentration water with high hardness and multiple ions by the EDIR process. Meanwhile, the different removal efficiencies of cationic ions were compared for a better understanding of the ion removal process. The feed solutions were simulated by dissolving the monovalent and divalent cation ions such as Ca^{2+}, Mg^{2+}, Na^+, and K^+. Various factors which influenced the EDIR performance were examined and optimized, including polarity reversal, flow rates, resin volume ratios, and operating currents. In addition, the competitive migration of cationic ions in this electro-membrane process was discussed and analyzed.

2. Experimental

2.1. Materials and analytical methods

In this study, commercial heterogeneous CM and AM, which were purchased from Shanghai Shanghua water treatment material Co. Ltd., China, were used as ion selective permeation media. The CM and AM containing sulfonic acid and quaternary ammonium groups, respectively, were specifically manufactured with low water permeability. The surface of the membranes was analyzed with energy-dispersive X-ray spectroscopy (EDS) which connected to a scanning electron microscope (SEM) S4800 from Hitachi High-Technologies Corporation, Japan. The macroporous cation and anion exchange resins, which were strongly acidic and basic types, named D072 and D296, respectively, were used as the ion exchange fillers. They were from Tianjin Hecheng S&T Develop Co. Ltd., China , with original sodium and chlorine forms, respectively. Table 1 shows the properties of ion exchange membranes and resins.

The synthetic solution was prepared by adding $CaCl_2$, $MgSO_4$, KCl, and Na_2SO_4 reagents with the same molar ratio of cationic ions into fresh deionized water, and its pH value was 5.4. The hardness of the solution was 800 mg L^{-1} as $CaCO_3$ (concentration range of hardness from the United States Geological survey), and mass concentrations of the cationic ions (Ca^{2+}, Mg^{2+}, Na^+, and K^+) were 160, 96, 92, and 156 mg L^{-1}, respectively. The specific conductance of solution was 2.16 mS cm^{-1}. The simulated solution in this study was designed to represent for the brackish water with high hardness. All the reagents used in this experiment were of analytical grade. Different ion mass concentrations in solution were measured by Varian 715-ES from Agilent Technologies, Inc., USA. The other measuring instruments were 2200 online pH Meter from Guangzhou Huigu Environmental Technology Co. Ltd., China; GLI online conductivity meter provided by Hach Water Quality Analysis Instrument (Shanghai) Co. Ltd.; and UA78A digital multimeter for cell voltage and resistance. The power appliance was TYP2500 booster pump from Deng Yuan Industrial Co. Ltd., and the electric power supply was TRP3003C-3R DC power from Shenzhen Atten Technology Co. Ltd., China.

Table 1
Characteristic properties of ion exchange membranes and resins

Items	Matrix structure	Resistance (Ω cm^2)	Selective penetration (%)	Exchange capacity (mmol g^{-1})	Moisture content (%)	pH range	Functionality
CM	Styrene−DVB	11	90	2	35–55	1–10	$-SO_3^-$
AM	Styrene−DVB	12	89	1.8	30–45	1–10	$-N^+(CH_3)_3$
D072	Styrene−DVB	[a]	[a]	≥4.4 (dry)	45–55	1–14	$-SO_3^-$
D296	Styrene−DVB	[a]	[a]	≥3.7 (dry)	50–60	1–14	$-N^+(CH_3)_3$

[a]Data not available.

2.2. Illustration of the EDIR stack

The EDIR configuration is schematically presented in Fig. 1. The dimension of each compartment was 45 cm × 3.5 cm × 0.5 cm, and the effective membrane area was 157.5 cm^2. The stack consisted of four packed compartments and two electrode compartments in all. And the four chambers with resins packed were numbered C-1, C-2, C-3, and C-4 from left to right. The feed stream had four flow passages into the compartments, and the flow directions were parallel with each other. At the outlet, lines from C-1 and C-3 will converge into one and the lines from C-2 and C-4 into another one. The nitric acid solutions with pH of 2 circulated during the experimental process as the electrode rinsing water. The electrode plates were made of ruthenium-coated titanium, and the electrode compartments were filled with four-layered nylon screens to ensure even flow distribution. Before the experiment, the resins were soaked in alcohol solutions for 96 h to dissolve impurities and followed by washing in deionized water until no alcohol remained and finally stored in deionized water for experiment. The same pretreatment method was applied to the membranes. Then, the cation and anion exchange resins were mixed and filled in the chambers at different volume ratios (i.e. the cation–anion ratio of 7:3, 4.7:5.3, and 3:7). When the polarity of the electrodes was reversed periodically in the EDIR operation, the ion migration changed directionally, and the DC and CC were interchanged.

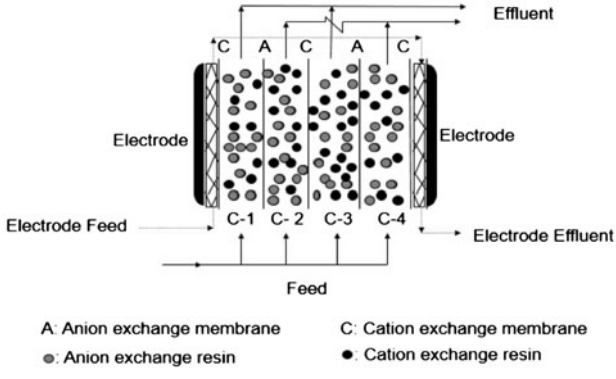

Fig. 1. Schematic representation of the EDIR stack.

The flow diagram of the EDIR setup is illustrated in Fig. 2. It consisted of an EDIR stack, two separate inflow lines, one electrode circulating stream, power supplier, measuring system, and water tanks. The feed solution was powered by the booster pumps and separated into two streams from the feed water tank. The effluent from the DC and CC was discarded through the online measuring instruments such as conductivity meters and pH meters which were installed on the outlet of each stream for monitoring the quality of water. The resistance of each compartment was detected by the digital multimeter at the resistance contacts. The electrode rinsing water circulated from the cathode to anode at the flow rate of 12 mL min^{-1}. Flow rates of the DC were regulated by the flow meter at the outlet, and the concentrate flow was maintained at 30 mL min^{-1}. The direct-current power supply was connected to the EDIR stack, and the electrode reversal processes were controlled by the reversal switch. The voltage and current of the EDIR stack were recorded during the experiment.

2.3. Operating conditions

Firstly, the *V–I*, *R–I*, and *R–T* (resistance vs. time) curves were achieved without polarity reversal to investigate the proper operating current and polarity reversal interval. Then, the operation was conducted under the condition of polarity reversal. In order to avoid the over-limiting current when the polarity was reversed, the EDIR stack was running at a constant current. It was conducted by setting the DC power supply to constant current mode, and then, the current was fixed at a certain value during the desalination process, while the voltage would change according to the variation of stack resistance to maintain the stable

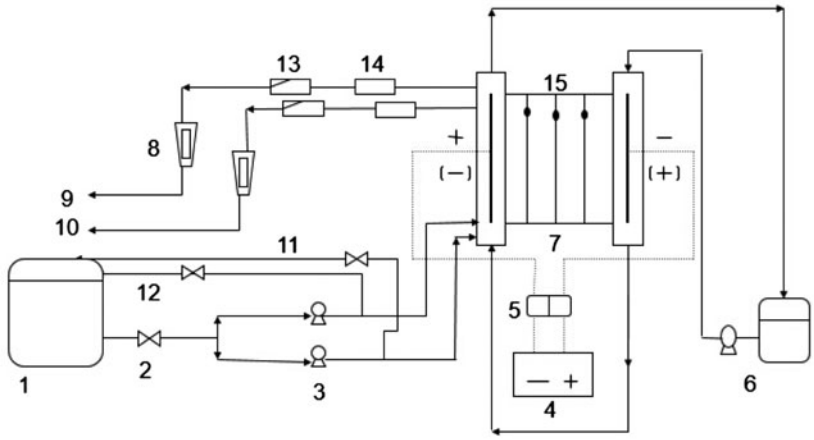

1. Feed water tank; 2. Controlling value; 3. Lift pump; 4. DC power; 5. Reversal switch; 6. Electrode water tank; 7. EDIR stack; 8. Flow meter; 9 and 10. Dilute or Concentrate effluent; 11 and 12. Backflow; 13. On-line conductivity meter; 14. On-line pH meter; 15. Resistance contacts

Fig. 2. Flow diagram of the EDIR system.

current. When the polarity was reversed by the reversal switch, the current remained constant, and the voltage would decrease at first and then increase to a stable range.

Different resin volume ratios (cation–anion, 7:3, 4.7:5.3, and 3:7) were investigated, and various flow rates of dilute stream were listed in Table 2. Only one parameter varied in each experiment, and performances of these experiments were recorded. All the experiments were carried out for three times, and their mean value was taken as the final result. Removal efficiency of each cation ion was calculated by the following Eq. (1):

$$R = \frac{C_{in} - C_{out}}{C_{in}} \times 100\% \quad (1)$$

where R is the removal efficiency of each cation ion, C_{in} is the feed concentration of each cation ion, and C_{out} is the effluent concentration of each cation ion.

3. Results and discussion

3.1. Operating current investigation

In Fig. 3, *V–I* and *R–I* curves for both DC and CC were presented. In the resin bed, the specific conductance has been investigated in porous plug model [21] that there exist three elements in parallel for the migration of ions to form electric current, namely (i) alternating layers of solution and resins, (ii) ion exchange resins, and (iii) solution. When the solution is more conductive than resins, current will be delivered mainly in the aqueous phase and the electromembrane process will exhibit some characteristics of ED process [22,23]. In this study, the conductivity of the feed water was relatively high, which might result in the characteristic of ED. From Fig. 3, the *V–I* curve of the DC could be divided into two sections: slope and plateau regions. In the slope region where the corresponding current was from 0.15 to 0.862 A, the value of resistance increased with current due to concentration polarization. Since almost no salt ions were available for electrical current transport, water began to

Table 2
Flow rates of batch experiments

Serial number	Dilute flow rate (mL min^{-1})	Concentrate flow rate (mL min^{-1})	Electrode flow rate (mL min^{-1})
E-1	15	30	12
E-2	30	30	12
E-3	60	30	12
E-4	90	30	12

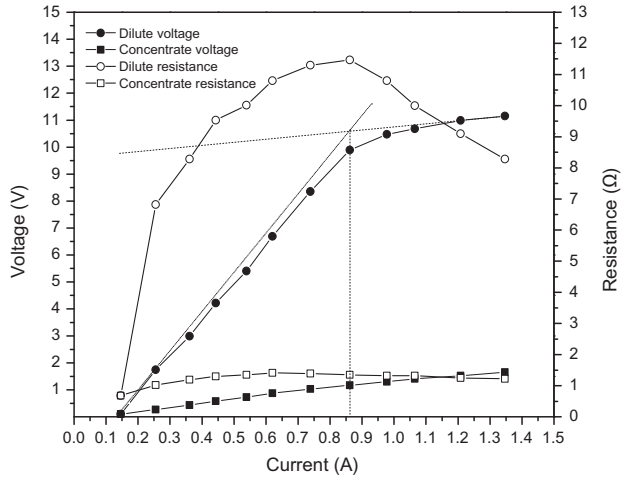

Fig. 3. *V–I* and *R–I* curves in the EDIR process.

dissociate. The water dissociation produced H^+ and OH^- which resulted in a drastic decrease in the stack resistance. Therefore, in the plateau region, (corresponding current from 0.862 to 1.35 A), a tendency of decreasing resistance was observed, which was revealed in the EDI process [4]. It was indicated that water dissociation had taken place and an increasing part of current was carried by the ionic products at the depletion layer of membranes and resins.

The point of intersection was determined where one plotted tangent lines at the beginning and the end of the *V–I* curve. Its corresponding current as critical value was 0.862 A. In the EDIR process, a certain degree of water dissociation should occur in the DC [19] in order to achieve good desalination performance and high current efficiency. The operating current was allowed to be over the critical value. While considering the high hardness and scaling formation, the operating current was chosen to be 0.85 A which could obtain a high current efficiency as possible.

As the ion species migrated continuously from the DC to the CC, the ionic concentration was constantly increasing in CC. Hence, compared with the DC, the CC provided much higher electrical conductivity. In Fig. 3, it was observed that the resistance of CC changed slightly and it can be concluded that the changes of the stack resistance were mainly affected by that of the DC.

3.2. Membrane scaling and polarity reversal interval

In electro-membrane process, scale deposition cannot be tolerated because of its highly deleterious effects on membranes and specific energy consumption. In order to control the effects of scaling on membrane, the fouling process in this experiment should be investigated. In this study, feed water contains scale forming ions which are prone to precipitate $CaCO_3$, $CaSO_4$, and $Mg(OH)_2$, etc. The precipitation is induced by the generation of a high pH environment on membrane surface, where the high alkaline environment acts to convert the HCO_3^- ion into the CO_3^{2-} form and the ensuing high super saturation level of $CaCO_3$ promotes its precipitation. The high pH conditions promote precipitation of $Mg(OH)_2$ as well.

In Fig. 4, the resistance change was displayed under the condition of constant current 0.85 A, and flow rate of 30 mL min^{-1} in DC. The cation–anion resin volume ratio was 4.3:5.7. The electrode polarity was not reversed in order to evaluate the status of precipitation. In the range of 0–60 min, the stack resistance decreased at a regular rate due to the increasing ion concentration in the CC. And then, the stack resistance gradually increased which might result from both concentration polarization and the precipitation on the surfaces of the resins and membranes in the DC. The scaling of membrane surface can be reflected through the resistance change because scaling formation on membrane surface will lead to the reduction of the effective area of membrane, and it can be seen that there was an obvious growing tendency over the period of 60–240 min, which might indicate that the precipitation began to deposit on the surface of ion exchange membranes, thus leading to the increased resistance. From Fig. 4, the reversal interval should be within 60 min, for the polarity reversal which could avoid or minimize scale formation.

After the experiment, the stack was disassembled to observe the status of the membrane surface and

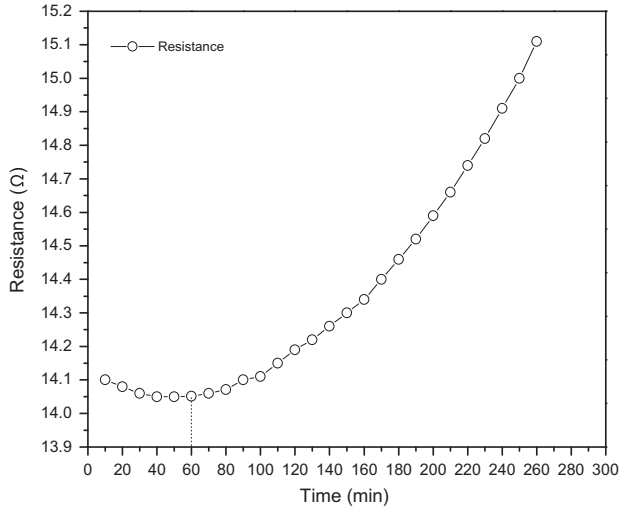

Fig. 4. *R–T* relationship at 0.85 A without polarity reversal.

precipitation was found on the surface of the CM. The SEM-EDS results were presented in Fig. 5(a); the main elements were shown in the EDS analysis. In the figure, the characteristic peak value could represent the mass amount of the element and it can be seen that the main elements on the membrane surface were Mg, O, C, S, and Ca according to the characteristic peaks. Thus, it can be concluded that the chemical compositions of the precipitation were $CaSO_4$, $Mg(OH)_2$, and carbonate of calcium and magnesium. For comparison, the CM image which was used after 13 h in condition of polarity reversal interval of 60 min, operating current 0.85 A, is presented in Fig. 5(b). As observed in the figure, almost no scale formation was seen on the membrane surface and the low content of Ca and Mg existed due to adsorption of CM when the experiment was ended. Then, the scale formation could be inhibited effectively with the reversal interval of 60 min.

In addition, it was investigated that the change of the electric polarity which prevented or minimized membrane fouling and scale was due to the pulsation effects on the membrane surface [16]. The reversal of polarity in electro-membrane process resulted in the opposite movement of ions under an electric field, minimizing the molecular binding for the scaling species, and thus disturbing the formation of the scale on the surface of membranes. Since reducing the period of the polarity change (i.e. the higher frequency) caused a higher pulsation effect on the membrane surface, it can be speculated that a shorter interval of polarity reversal would have better precipitation preventing performance for a stable and reliable operation of the electro-membrane systems.

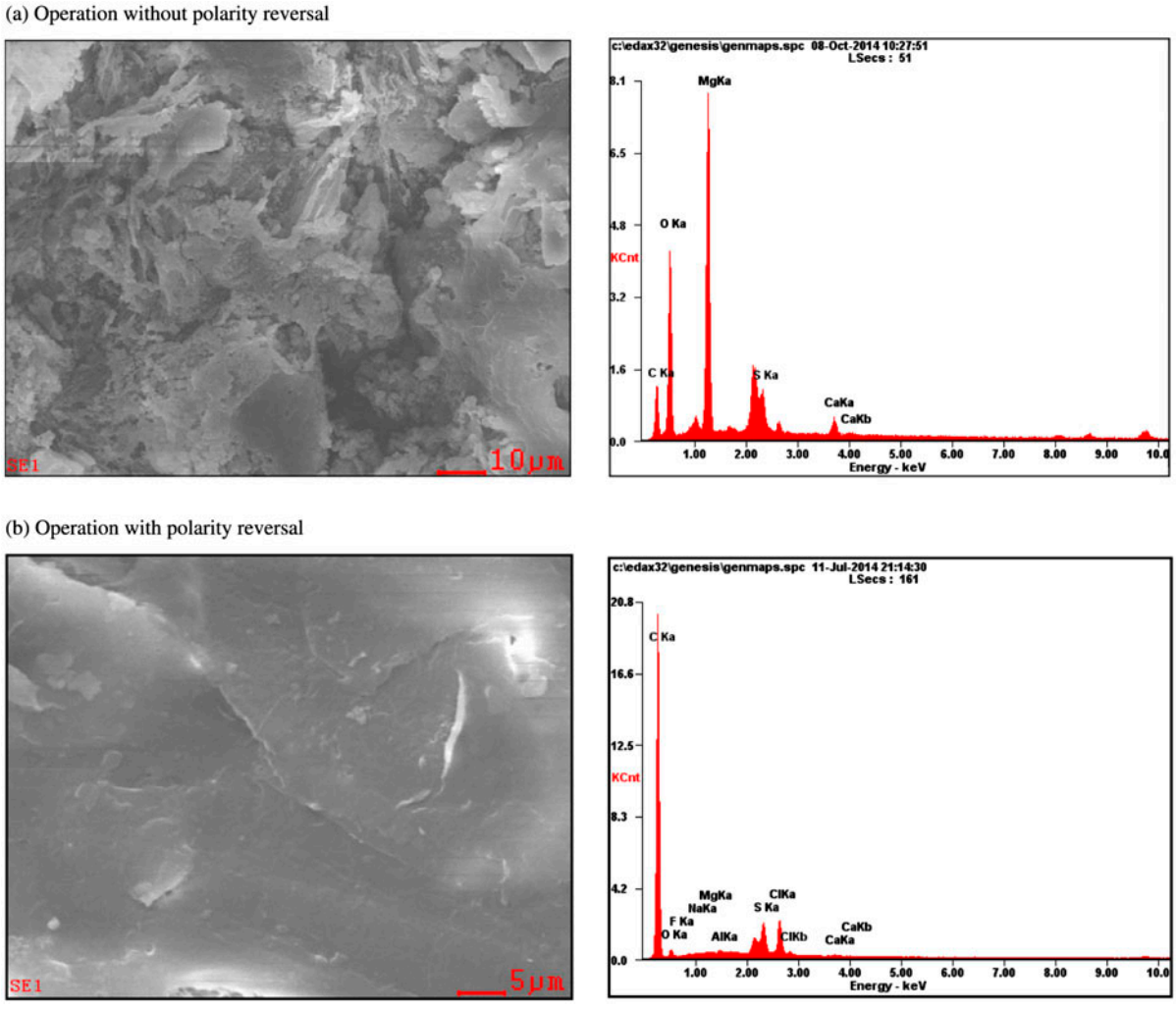

Fig. 5. Analysis of scaling on the cation membrane surface using SEM-EDS.

3.3. Specific conductance of effluent with polarity reversal

The specific conductance of the effluent streams as a function of operation time was plotted in Fig. 6. Periodic interval was set to 60 min, and the resin volume ratio of cation–anion was 4.3:5.7. The parameters of flow rates (E-2) were recorded in Table 2, and the constant operating current was 0.85 A. In EDIR system, the effluent of DC in a previous periodic period would turn to be the concentrate effluent when the polarity was reversed. The conductive changes of the effluent from C-1 to C-3 vs. time were presented in Fig. 6(a); it can be seen that the conductivity evidently followed an alternating increase-decrease trend after the start-up of the stack, which meant that the effluent from C-1 and C-3 interconverted between the dilute stream and concentrate stream due to the periodic change of electrodes. For C-2 and C-4, the corresponding dilute-concentrate process is shown in Fig. 6(b).

In Fig. 6(c) and (d), the conductivity changes of the DC and CC were displayed. It was observed that the value of conductivity would remain in a relatively stable range that the conductivity of dilute effluent was 0.55–0.105 mS cm^{-1} and the conductivity of concentrate effluent was 4.41–4.75 mS cm^{-1}. However, in every periodic period, a maximum conductivity value of the dilute effluent and a minimum conductivity value of the concentrate effluent would be achieved after polarity reversal. Taking the concentrate effluent conductivity as analysis object, the curves increased obviously in the first 60 min and had a rapid

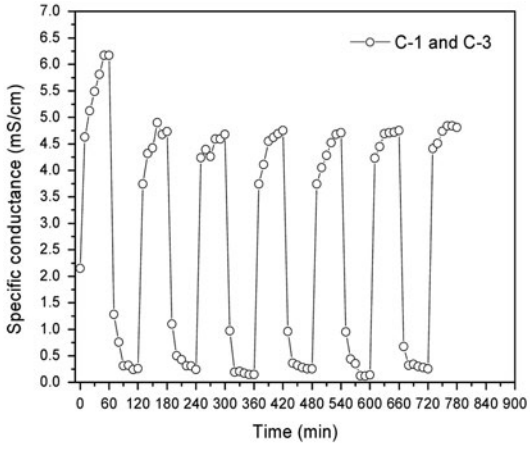

(a) Effluent conductivity of C-1 and C-3 versus time

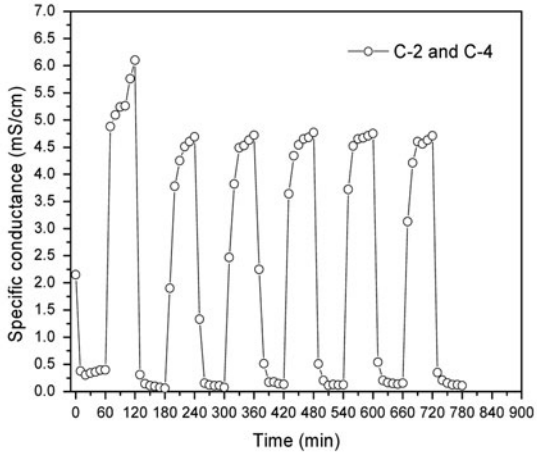

(b) Effluent conductivity of C-2 and C-4 versus time

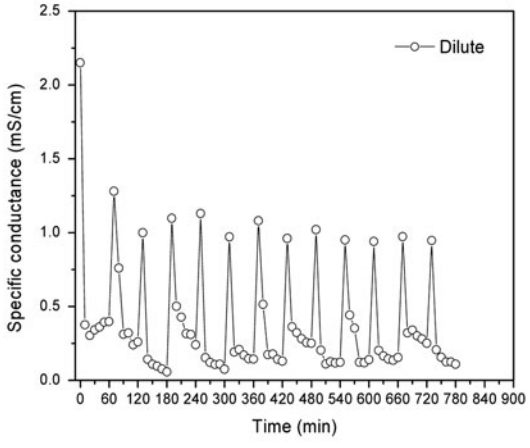

(c) Effluent conductivity of the DC versus time

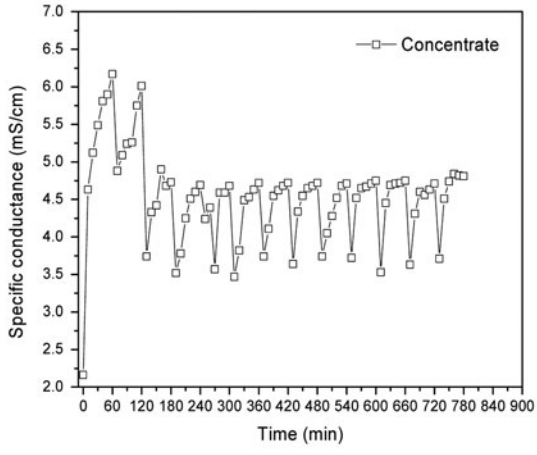

(d) Effluent conductivity of the CC versus time

Fig. 6. Specific conductance of effluent with polarity reversal.

decrease at the beginning of next period. And then, it kept durative increasing in the later 50 min until the conductivity value remained stable around 4.51 mS cm^{-1}. This periodic change of conductivity appeared in every polarity reversal period. These results were because the feed stream entering the new CC which was previous DC as the polarities were reversed, and the salt ions were brought out from the previous CC by the concentrate effluent before being transferred into DC in the electric field, thus leading to the instantaneous decrease in conductivity. And the corresponding change occurred to the dilute stream as well.

Moreover, from Fig. 6 ((a)–(d)), it can be discovered that the stable conductivity range in 0–120 min was obviously higher than that of the later periods. The higher conductivity value in the first 120 min was mainly involved with the substitution of previous Na^+ due to the higher ion affinity and selectivity with Ca^{2+}, Mg^{2+}, and K^+ ions of the ion exchange resins. For the cation exchange, membranes and resins were both originally in Na-form, Ca^{2+}, Mg^{2+}, and K^+ ions from the feed water could exchange with Na^+ in cation exchange resins as they entered both the DC and CC. Thus, the outlet Na^+ concentration was relatively high. As a result, the effluent was more conductive than that of the later periods due to the higher mole conductivity of Na^+. From Fig. 6, it was indicated that the replacement of original Na^+ ion took about 120 min. Furthermore, in the later periods, by comparing the conductivities of the feed water and effluent, it was found that the total conductivity of the effluent (dilute and concentrate) in unit time was higher than that of the feed water, which indicated that some ion species more conductive were generated. It can be explained by the water dissociation in DC. When the salt concentration at the depletion layer reached a sufficiently low level, water dissociation took place and a significant part of current was carried by the ionic products, H^+ and OH^-. However, there were differences between the AM and CM. Simons [22] considered that the dissociation phenomena was the essential characteristic of AM containing tertiary amine groups and water dissociation on the CM would be accelerated rapidly when Ca^{2+} and Mg^{2+} ions were in the solution as electrolytes. Hence, in this experiment, the water dissociation should be taken into account. As the operating current was not beyond the critical value, the water dissociation was mainly accelerated by the existence of Ca^{2+} and Mg^{2+} ions on the surface of CM. The H^+ with much higher mole conductivity than other ions migrated through the CM to the CC, thus resulting in the increased conductivity of the concentrate effluent.

3.4. Influences of flow rates and resin volume ratios on EDIR performance

The influence of various dilute flow rates on EDIR performance was displayed in Fig. 7. Four different dilute flow rates (15, 30, 60, and 90 mL min^{-1}) were selected for this examination. Similar trend of development of dilute conductivity during the operation was observed, and effluent conductivity decreased with voltage at each fixed feed flow rate. From Fig. 7, the effluent conductivity of different flow rates followed such an order: $90 > 60 > 30 > 15$ mL min^{-1}. It can be observed that the outlet conductivity was getting lower and lower with the decreasing flow rates, which indicated that the residence time was getting longer for the cation ions to contact with ion exchange resins, thus more ionic species were removed and a better performance was exhibited.

However, the effluent conductivities of 30–15 mL min^{-1} did not have a significant difference. This was caused by the hydrodynamic effect: The diffusion layer thickness of ion exchange resins increased, and crossing the diffusion layer into resins became the slowest step when the ions were moving from DC to CC. Although the flow rate of 15 mL min^{-1} could prolong the residence time for ions, the ion removal efficiencies were nearly the same with that of 30 mL min^{-1}, implying that the diffusion layer thickness was increased, thus the removal efficiency was affected. As to the higher flow rates of 60–90 mL min^{-1}, the increasing flow rates resulted in decreasing the thickness of the diffusion layer as well as the residence time. Hence, the removal efficiencies were relatively low. By comparison, the 30 mL min^{-1} was proper for its high removal performance and less influence from the

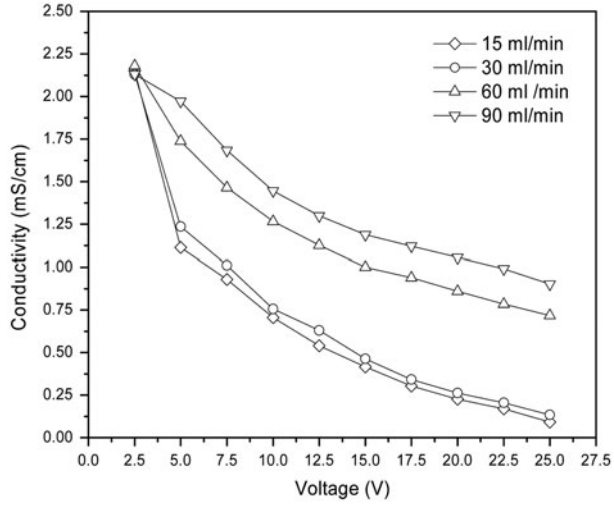

Fig. 7. Influences of flow rates on EDIR performance.

diffusion layer than that of 15 mL min^{-1}. And also, it was indicated that the removal efficiency could be high if the residence time was long enough especially for the high-concentration feed.

In Fig. 8, the effluent pH and conductivity of DC with different resin volume ratios were displayed. The operating condition was reversal interval of 60 min, operating current at 0.85 A, and the ratios (cation–anion) were 7:3, 4.7:5.3, and 3:7. Dilute flow rate was 30 mL min^{-1}. It can be seen that the pH of the effluent was quite different with various resin volume ratios, which indicated that water dissociation occurred on the membrane surface. In further observation, the pH of the DC was alkalescent in the ratio of 3:7 (cation–anion). Since the anion exchange resins were more than twice of the cation exchange resins, there existed a higher conductivity channel for anions than that of cations. Thus, the migration of anions was much more improved, and the transport number of anions in DC was far larger than that of cations. Anion concentration on the surface of the AM was much higher than that of cations on the CM, and then, the depletion region on CM appeared, which resulted in concentration polarization and water dissociation. The products, H^+ and OH^-, were transported as the current. The H^+ migrated across CM, while OH^- turned to the opposite direction [24] and migrated toward the AM in DC, thus making the DC alkaline. As for the ratio of 7:3 (cation-anion), the reason for the acidic effluent can be explained by the enhanced migration of cations and the concentration polarization resulting in water dissociation on the dilute side of the AM. The proper ratio was 4.3:5.7 (cation–anion), and it was determined according to the total mass ratio of cations and anions. The transport numbers of cations and anions were close to each other, and the concentration polarization on membrane surface could be alleviated. Thus in the electric field, the effective migration of cations and anions was enhanced to similar extent which was beneficial to avoid concentration polarization on membrane and moderate the pH of effluent to normal range.

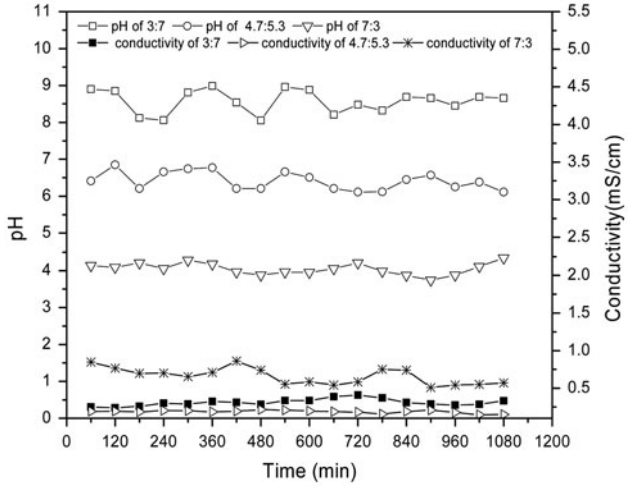

Fig. 8. Influences of resin volume ratios (cation–anion) on EDIR performance.

Thus, it can be concluded that the ratios of resins could affect the transport of cations and anions in the electro-migration process as well as tendency of water dissociation on membranes, which would result in the changes of effluent pH.

Similarly, the water quality was also relevant to various resin ratios. The effluent conductivity of the resin ratio of 4.7:5.3 was in the range of 0.105–0.21 mS cm^{-1}, while the conductivity of resin ratio 3:7 was 0.24–0.41 mS cm^{-1}. The highest effluent conductivity range was 0.51–0.86 mS cm^{-1} when the cation–anion volume ratio was 7:3. Due to improper ratio of resins, concentration polarization occurred on membrane surface, resulting in removal efficiency decrease. Thus, in Fig. 8, the ratio of 4.7:5.3 had better performance on ion removal than that of the other two ratios. The resin volume ratio should be in a proper range in order that the cations and anions were transferred equally. Hence, the migration of ions was effective, and current efficiency was relatively high.

3.5. Competitive migration in EDIR process

As for the brackish water, multiple ions coexist in the aqueous phase and they will migrate simultaneously under the force of applied voltage. The removal of a particular ion will be affected by the presence of other similar ions (Ca–Mg and Na–K). Moreover, different valence states (monovalent and bivalent) of ions also impact the migration in the electro-membrane process. As discussed in 3.1, there are three kinds of migration paths for ions in the resin bed. Thus, the competition among these ions for the migration paths as well as ion mobility in transmission medium will affect their removal efficiencies.

In Fig. 9(a), it showed the removal efficiency as a function of various operating currents, and it was seen that removal efficiencies all increased with current which meant that the increasing electric field resulted in intense migration of ions, and thus, more ions were removed. In Fig. 9(b) and (c), the mass concentration within a single reversal period and the removal efficiencies under the constant current 0.85 A were plotted. The polarity reversal interval was 60 min, and the

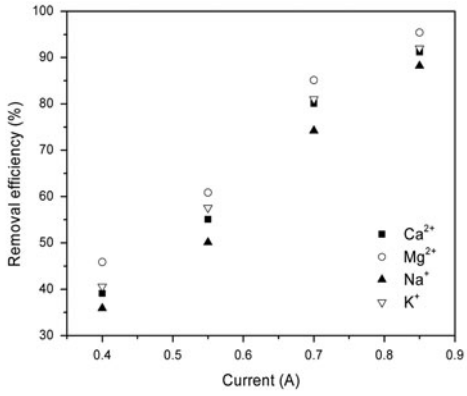

(a) Ion removal efficiencies with different currents.

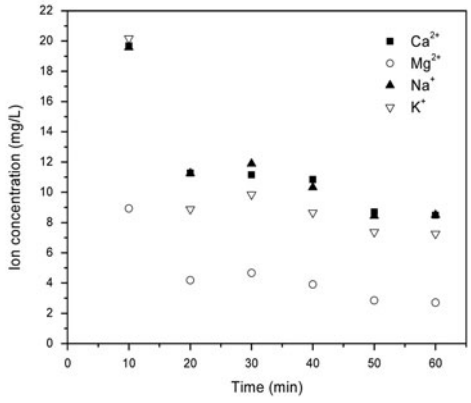

(b) Ion concentration change during a single polarity reversal period of 60 min.

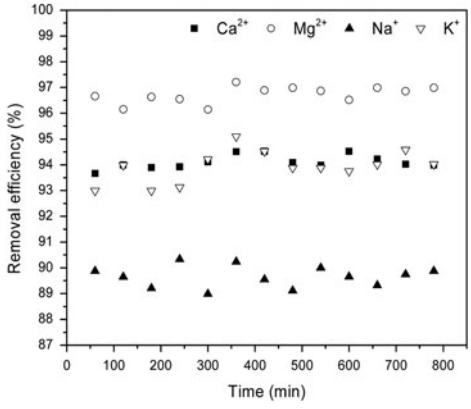

(c) Ion removal efficiencies in constant current 0.85A.

Fig. 9. Ion removal efficiencies in EDIR process.

dilute flow rate was 30 mL min^{-1}. It was observed that the removal efficiency of Mg^{2+} was the highest, Ca^{2+} and K^+ were close to each other, and Na^+ was the lowest. The total removal efficiencies were 93.12–94.56% for Ca^{2+}, 96.21–97.14% for Mg^{2+}, 89.11–90.76% for Na^+, and 92.99–95.35% for K^+.

It is known that ion exists in the state of hydrated form in solutions and the hydrodynamic radius, the effective radius for the migration of ions taking into account the entire object that moves, is affected by the ionic radius and electrostatic charge. Ions with smaller intrinsic crystal radii have higher hydration numbers, larger hydrated radius, and hold their hydration shells more strongly, as listed in Table 3. The larger the crystal ionic radius, the more diffuse the electric charge and the fewer water molecules surround the ion [25]. In this study, the hydration radius order was $Mg^{2+} > Ca^{2+} > K^+ > Na^+$. Meanwhile, ion affinity and selectivity could be partly explained by considering the ion valence. The affinity is proportional to ionic charge. A larger ionic charge means a stronger electrostatic interaction with ion, and thus, the Ca^{2+} and Mg^{2+} were adsorbed preferentially and then K^+ and Na^+. In the interior of resin, the ion which had already adsorbed on the site of functional groups ($-SO_3^-$) by electrostatic interactions would break away due to the electric force from the electrode and move to the direction of the electrode through ion exchange membrane, leaving a vacancy on the site of functionalities. The ions nearby would cover the position by the coinstantaneous force of electric field and static. Thus under the dual forces, the ion migration was accelerated through the high conductivity channel composed of sites on functional groups. The migration of Na^+ on the sites of functionalities in resin for example was illustrated in Fig. 10.

Comparing the removal efficiencies of Ca^{2+} and K^+, it can be speculated that the transport number of Ca^{2+} was bigger than that of K^+ in the resin phase, for K^+ ions has a higher ion mobility in aqueous phase than Ca^{2+}. As for Na^+, the transport number might be the lowest in resin phase due to competitive adsorption to resins and it migrated mainly in solution. The migration of Mg^{2+} was the most effective due to the relative high removal efficiency.

After comparing the ion mobility in Table 3, it can be concluded that the migration of Mg^{2+} and Ca^{2+} was accelerated more than that of K^+ and Na^+ in the conductivity channel of resins due to the preferential affinity of ion exchange resins. As for Mg^{2+} and Ca^{2+}, Mg^{2+} had larger hydrated radius, which indicated that the positive charge center was farther from the site of functional group and the resin-site electrostatic interaction from the previous site of functional group would be weaker during the migration process. Thus, the retarding force it experienced from the electrostatic attraction of the functional groups was weaker than Ca^{2+}. Hence, the migration rate in resins of Mg^{2+} was faster than that of Ca^{2+}. It can be concluded that the transport number of Mg^{2+} in resin phase was the

Table 3
Characteristics of cation ions

Parameter	Ca^{2+}	Mg^{2+}	Na^{+}	K^{+}	References
Crystal ionic radii (nm)	0.1005	0.072	0.1011	0.1377	[26]
Hydrated ionic radii (nm)	0.260	0.300	0.178	0.201	[27]
Hydration number	8.5	8	5.9	6.6	[28]
Ion mobility ($10^{-8}m^2s^{-1}V^{-1}$) at 298 K	6.17	5.5	5.19	7.62	[29]

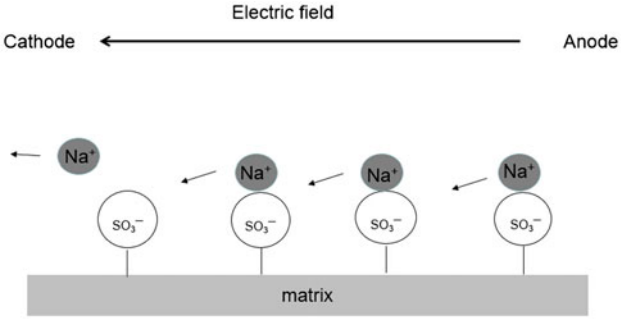

Fig. 10. Ion migration on functional sites in resin phase.

biggest followed by that of Ca^{2+}, while the migration of K^{+} and Na^{+} was mainly in aqueous phase due to preferential adsorption to resins of Ca^{2+} and Mg^{2+}.

4. Conclusion

In this study, an EDIR process for desalination of high hardness water was employed. Optimum conditions (operating current of 0.85 A, polarity reversal interval within 60 min, dilute flow rate of 30 mL min^{-1}, and cation–anion resin volume ratio of 4.3:5.7) were determined experimentally. The conductivity in feed water could be decreased from 2.16 to 0.105 mS cm^{-1} (i.e. a conductivity removal efficiency of 95.1%), and the removal percentages of cationic ions were 93.12–94.56% for Ca^{2+}, 96.21–97.14% for Mg^{2+}, 89.11–90.76% for Na^{+}, and 92.99–95.35% for K^{+}. Herein, a high-efficient desalination process without membrane scaling was achieved. In addition, it was concluded that the removal efficiency of Mg^{2+} was higher than that of Ca^{2+}, K^{+}, and Na^{+} during this electromembrane process.

Thus, it is shown in this study that the EDIR could be considered as a potential technology for the desalination of high-concentration water, and this study will also be helpful for understanding the multi-ion removal process in EDIR.

Symbols

R	—	removal efficiency (%)
C_{in}	—	feed concentration (mg L^{-1})
C_{out}	—	effluent concentration (mg L^{-1})

References

[1] R. Kunin, R.J. Myers, Ion Exchange Resins, Wiley, New York, NY, 1950.
[2] Ö. Arar, Ü. Yüksel, N. Kabay, M. Yüksel, Various applications of electrodeionization (EDI) method for water treatment—A short review, Desalination 342 (2014) 16–22.
[3] G.C. Ganzi, Y. Egozy, A.J. Giuffrida, High purity water by electrodeionization: Performance of the Ionpure continuous deionization system, Ultrapure Water 4 (1987) 43–50.
[4] J.H. Song, K.H. Yeon, S.H. Moon, Effect of current density on ionic transport and water dissociation phenomena in a continuous electrodeionization (CEDI), J. Membr. Sci. 291 (2007) 165–171.
[5] J. Wood, J. Gifford, J. Arba, M. Shaw, Production of ultrapure water by continuous electrodeionization, Desalination 250 (2010) 973–976.
[6] J. Lu, Y.X. Wang, Y.Y. Lu, G.L. Wang, L. Kong, J. Zhu, Numerical simulation of the electrodeionization (EDI) process for producing ultrapure water, Electrochim. Acta 55 (2010) 7188–7198.
[7] V.I. Fedorenko, Ultrapure water production by continuous electrodeionization method: Technology and economy, Pharm. Chem. J. 38 (2004) 35–40.
[8] L. Alvarado, I.R. Torres, A. Chen, Integration of ion exchange and electrodeionization as a new approach for the continuous treatment of hexavalent chromium wastewater, Sep. Purif. Technol. 105 (2013) 55–62.
[9] Ö. Arar, Ü. Yüksel, N. Kabay, M. Yüksel, Application of electrodeionization (EDI) for removal of boron and silica from reverse osmosis (RO) permeate of geothermal water, Desalination 310 (2013) 25–33.
[10] P. Yu, Z. Zhu, Y. Luo, Y. Hu, S. Lu, Purification of caprolactam by means of an electrodeionization technique, Desalination 174 (2005) 231–235.
[11] R. Berrocal, M. Chaveron, Demineralization of milk and milk derived products by electrodeionization, US Patents No. 6033700, 2000.
[12] A.D. Khoiruddin, I.N. Widiasa, I.G. Wenten, Removal of inorganic contaminants in sugar refining process using electrodeionization, J. Food Eng. 133 (2014) 40–45.

[13] J.S. Park, J.H. Song, K.H. Yeon, S.H. Moon, Removal of hardness ions from tap water using electromembrane processes, Desalination 202 (2007) 1–8.
[14] A.J. Giuffrida, G.C. Ganzi, O. Yoram, Electrodeionization apparatus and module, US Patent No. 4956071, 1990.
[15] Y. Oren, Y. Egozy, Studies on polarity reversal with continuous deionization, Desalination 86 (1992) 155–171.
[16] H.J. Lee, J.H. Song, S.H. Moon, Comparison of electrodialysis reversal (EDR) and electrodeionization reversal (EDIR) for water softening, Desalination 314 (2013) 43–49.
[17] H.J. Lee, M.K. Hong, S.H. Moon, A feasibility study on water softening by electrodeionization with the periodic polarity change, Desalination 284 (2012) 221–227.
[18] Y. Zhang, L. Wang, S. Xuan, X. Lin, X. Luo, Variable effects on electrodeionization for removal of Cs^+ ions from simulated wastewater, Desalination 344 (2014) 212–218.
[19] H. Lu, Y. Wang, J. Wang, Removal and recovery of Ni^{2+} from electroplating rinse water using electrodeionization reversal, Desalination 348 (2014) 74–81.
[20] Ö. Arar, Ü. Yüksel, N. Kabay, M. Yüksel, Demineralization of geothermal water reverse osmosis (RO) permeate by electrodeionization (EDI) with mixed bed configuration, Desalination 342 (2014) 23–28.
[21] K.S. Spiegler, R.L. Yoest, M.R.J. Wyllie, Electrical potentials across porous plugs and membranes, ion-exchange resin-solution system, Discuss. Faraday. Soc. 21 (1956) 174–183.
[22] R. Simons, Water splitting in ion exchange membranes, Electrochim. Acta 30 (1985) 275–282.
[23] F. Maletzki, H.W. Rösler, E. Staude, Ion transfer across electrodialysis membranes in the overlimiting current range: Stationary voltage current characteristics and current noise power spectra under different conditions of free convection, J. Membr. Sci. 71 (1992) 105–116.
[24] H.D. Hurwitz, R. Dibiani, Experimental and theoretical investigations of steady and transient states in systems of ion exchange bipolar membranes, J. Membr. Sci. 228 (2004) 17–43.
[25] B. Tansel, J. Sager, T. Rector, J. Garland, R.F. Strayer, L. Levine, M. Roberts, M. Roberts, M. Hummerick, J. Bauer, Significance of hydrated radius and hydration shells on ionic permeability during nanofiltration in dead end cross flow modes, Sep. Purif. Technol. 51 (2006) 40–47.
[26] F. David, V. Vokhmin, G. Ionova, Water characteristics depend on the ionic environment, J. Mol. Liquids. 90 (2001) 45–62.
[27] M.Y. Kiriukhin, K.D. Collins, Dynamic hydration numbers for biologically important ions, Biophys. Chem. 99 (2002) 155–168.
[28] H. Binder, O. Zschornig, The effect of metal cations on the phase behavior and hydration characteristics of phospholipid membranes, Chem. Phys. Lipids 115 (2002) 39–61.
[29] P. Atkins, The Elements of Physical Chemistry With Applications in Biology, W.H. Freeman and Company, New York, NY, 2000.